ARTICLE IN PRESS

Available online at www.sciencedirect.com

ScienceDirect

Advances in Space Research xxx (xxxx) xxx

ADVANCES IN SPACE RESEARCH (a COSPAR publication)

www.elsevier.com/locate/asr

Investigation of the impact of Ionospheric Scintillation on GNSS Performance over East Africa

Faustine Abiriga [a,*], Emirant B. Amabayo [b], Edward Jurua [a], Pierre J. Cilliers [c]

[a] Department of Physics, Mbarara University of Science and Technology, Mbarara, Uganda
[b] Department of Physics, Busitema University, Tororo, Uganda
[c] South African National Space Agency (SANSA) Space Science, Hermanus, South Africa

Received 11 September 2020; received in revised form 9 May 2021; accepted 12 May 2021

Abstract

In recent decades, the reliance on Global Navigation Satellite System (GNSS) applications is gaining ground in the East African region. This region lies within the low geomagnetic latitudes where signal scintillation events due to ionospheric irregularities are frequent. Signal scintillation events pose a considerable challenge to the carrier tracking loop of a Global Positioning System (GPS) receiver's phase locked loop (PLL) and can result in cycle slips or even a total loss-of-lock. The cycle slips can degrade and disrupt satellite-based navigation systems, leading to significant positioning errors. In this study, data from the International GNSS Service (IGS) and SCIntillation Network and Decision Aid (SCINDA) for the year 2011 was used to statistically analyse the effects of ionospheric scintillation on satellite-based navigation over the East African region. Results obtained show that signal scintillation events follow a seasonal pattern with a higher percentage occurrence of amplitude scintillation events over phase scintillation events. Using the method of phase combinations, cycle slips were identified on GPS L-band signals. It was observed that the frequency of occurrence of cycle slips is higher on L2-frequency than on L1-frequency of the L-band. Furthermore, results showed that the presence of signal scintillation events in signal ray paths increased the errors in GPS receiver position measurement by up to about 10 m. This can compromise the reliability and accuracy of GPS applications in navigation.
© 2021 Published by Elsevier B.V. on behalf of COSPAR.

Keywords: Ionospheric irregularities; Ionospheric scintillation; Global navigation satellite system; Loss-of-lock; GPS Position measurement error

1. Introduction

Loss-of-lock (LL) and signal loss due to L-band signal scintillation events are by-far the most challenging effects of the Earth's ionosphere on the operations of GNSS applications (Klobuchar, 1991; Jiao et al., 2014). The signal scintillation events caused by ionospheric irregularities are predominant in high-latitude ($\geqslant \pm 65^\circ$ of the geomagnetic equator) and low-latitude ($\leqslant \pm 20^\circ$ of the geomagnetic equator) regions, particularly during solar maxima (Sreeja et al., 2011). The irregularities are less frequent in mid-latitude ($\pm 20^\circ$ to $\pm 65^\circ$ of the geomagnetic equator) regions. The ionospheric irregularities in high-latitude regions have been associated with transient solar events such as geomagnetic storms, while in low-latitude sector, the ionospheric irregularities have been associated with plasma drifts, neutral winds and pre-reversal enhancement (PRE) of the equatorial eastward electric field (Aarons et al., 1996; Du et al., 2000; Strangeways et al., 2011). These factors that lead to ionospheric irregularities in the low-latitude regions are predominantly post sunset events, and are not primarily driven by the transient solar activities since they can even occur during geomagnetically quiet

* Corresponding author.
E-mail addresses: abifaus@gmail.com (F. Abiriga), ejurua@must.ac.ug (E. Jurua), pjcilliers@sansa.org.za (P.J. Cilliers).

https://doi.org/10.1016/j.asr.2021.05.012
0273-1177/© 2021 Published by Elsevier B.V. on behalf of COSPAR.

times (Sreeja et al., 2011). These differing factors that lead to the occurrence of ionospheric irregularities in the different geomagnetic regions can be linked to the type of signal scintillation events that dominate the regions.

Many studies on ionospheric signal scintillation events (e.g. Aarons et al., 1996; Skone et al., 2005; Yizengaw et al., 2013) have been conducted in different parts of the world owing to the great impact scintillation events can have on GNSS receiver signal tracking performance. They can also impact the accuracy of GPS receiver position measurement estimates. In high-latitude regions, the predominant phase scintillation events can induce rapid phase shifts that may exceed the phase locked loop (PLL) bandwidth of the GNSS receiver, resulting in a loss of phase lock (Leick, 1995). Phase scintillation is characterized by scintillation index, σ_ϕ, which is the standard deviation of the signal carrier phase and is given by the expression (Van Dierendonck and Arbesser-Rastburg, 2004; Beach, 2006),

$$\sigma_\phi = \sqrt{\langle \Phi^2 \rangle - \langle \Phi \rangle^2}, \quad (1)$$

where Φ is the de-trended carrier phase of the GNSS signal; and $\langle\rangle$ indicates the average over a time interval of typically 60 s.

In low latitudes, amplitude scintillation is predominant and can cause the signal-to-noise ratio (SNR) to drop below the receiver's fading depth threshold, leading to signal loss and occurrence of cycle slips (Jiao et al., 2014). The cycle slips present sudden jumps in the carrier phase observables in GPS measurements by a multiple of integer number of cycles (Leick, 2004). These sudden jumps may occur independently on each or both of the L-band carrier frequencies. Amplitude scintillation is characterized by scintillation index, S4, which is the standard deviation of the received signal power measured at 50 samples per second, normalized over its mean value. Amplitude scintillation index, S4, is given by the expression (Briggs and Parkin, 1963; Datta-Barua et al., 2003),

$$S4 = \sqrt{\langle I^2 \rangle - \left\langle \frac{I}{\langle I \rangle^2} \right\rangle}, \quad (2)$$

where I is the intensity (power) of the signal and is computed by $I = A^2$; A denotes the amplitude of the signal.

The ionospheric behaviour over the East African low-latitude region is characterized by intense irregularities that can cause signal scintillation and occurrence of cycle slips on carrier phase measurements (Conker et al., 2003). The existence of cycle slips on carrier phase measurements can significantly influence the quality of GPS receiver position estimates. Apart from ionospheric scintillation events, other factors that can lead to the occurrence of cycle slips in carrier phase measurements include the malfunctioning of a receiver's software and/or hardware, multipath and line-of-sight signal obstructions by obstacles like tall buildings, forests and mountains (Skone et al., 2001; Hofmann-Wellenhof et al., 2007). All these factors increase the dilution of precision due to inefficient geometry of visible satellites. This affects the reliability and accuracy of GNSS applications in navigation and surveying (Banville et al., 2010). It also impacts ionospheric total electron contect (TEC) calculation (Yue et al., 2011).

Previous studies (e.g. Olwendo et al., 2013,Amabayo et al., 2014; Mungufeni et al., 2015) focussed on the occurrence of ionospheric irregularities and signal scintillation over the East African low latitude region, but did not pay attention to cycle slips and the impact of signal scintillation events on navigation and surveying. Since a cycle slip presents a discontinuity on a measured carrier phase due to transient LL in the tracking loop of a GNSS receiver (Yue et al., 2016), it limits the accuracy of position measurements by GNSS users. As a result, different studies (e.g. Donghyun and Langley, 2001; Hofmann-Wellenhof et al., 2007; Banville et al., 2010) developed different methods for detecting and repairing cycle slips. Such methods for detecting cycle slips include phase and code range combinations, doppler integration, differentials of phases with respect to time, and phase combinations. Fortunately, cycle slips arising from line-of-sight obstructions and multipaths can be avoided by setting high receiver mask elevation angles ($\geqslant 20^\circ$), depending on the location of the receiver (Mungufeni et al., 2015). In addition, some of the modern receivers are designed with the capability of dynamically changing the PLL bandwidth to allow for continuous tracking of the carrier phase (Humphreys et al., 2005). However, the challenge associated with the dynamically changing PLL bandwidth is that it is also associated with larger noise measurement, which can still degrade the performance of GNSS applications. In this study, we examined the statistics of occurrence of scintillation induced cycle slips on the different GPS L-band frequencies over the East African region using 2011 GPS data obtained from some selected International GNSS Service (IGS) and University NAVstar COnsortium (UNAVCO) receiver stations located in the region. Furthermore, we analyzed the effect of ionospheric irregularities on GNSS user position measurements in the region using parameters obtained from SCINDA data collected from SCINDA receivers in the same region for the same period.

2. Data sources and processing

The 2011 GPS and scintillation data used in this study were obtained from IGS and SCINDA receiver stations located within the East African region as shown in Fig. 1. The year 2011 was selected because it was on the ascending side of solar cycle 24, one of the weakest solar cycles in centuries (https://earthsky.org/space/solar-cycle-24-25-sunspot-predictions). This period was ideal for this study because the ionospehere had less agitations from solar activities. In addition, for the first time, both GPS and scintillation data could be obtained from IGS and

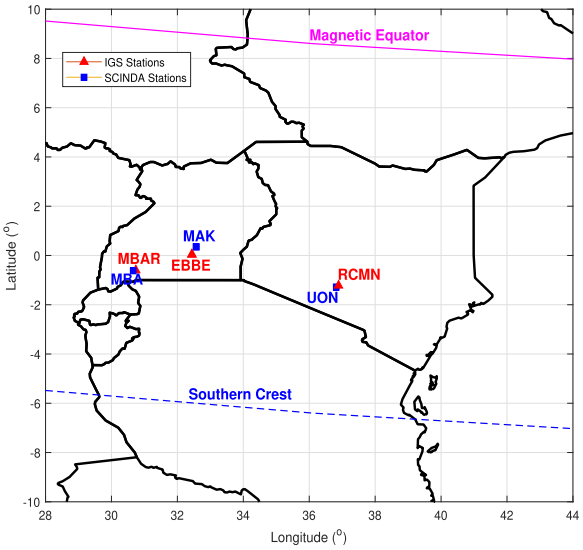


Fig. 1. Map of East Africa showing the locations of the selected IGS and SCINDA receiver stations from which the data used in this study was obtained.

SCINDA receiver stations installed within this region of study. The GPS data, contained in Receiver INdependent EXchange (RINEX) file format, was downloaded from Crustal Dynamics Data Information System (cddis) data centre via ftp://cddis.gsfc.nasa.gov from IGS receivers with station codes RCMN, MBAR and EBBE located in Nairobi (Kenya), Mbarara and Entebbe (in Uganda), respectively. The scintillation data, contained in ionospheric scintillation monitor (ism) format, was obtained from SCINDA receivers with station codes MBA, MAK and UON located at Mbarara University of Science and Technology, Makerere University and University of Nairobi, respectively. The choice of these IGS and SCINDA receiver stations was based on the fact that their locations were close to each other. The distances between the IGS and SCINDA receivers are: MBAR to MBA is 9.2 km, EBBE to MAK is 37.2 km and RCMN to UON is 10.2 km.

Table 1 presents the geographic and geomagnetic latitudes, and the geographic longitudes of the selected receiver stations used in this study. The number of days for which the stations had data available for analysis and the resolution of the data are also presented in Table 1. The geomagnetic latitudes for epoch 2011 were calculated using the APEX model, obtainable at https://www.ngdc.noaa.gov/geomag/geom_util/apex.shtml. Occasional system outages due to hardware, software or environmental issues led to missing data during this period of study. This explains why in Table 1, the IGS receiver station at Entebbe (EBBE) was the only one that collected data throughout the year, presenting 365 days of data. The rest of the receiver stations presented fewer days with data, hence data gaps. Fig. 2 summarizes the distribution of data collected per receiver station by analysing the number of days during which data was recorded in each month.

2.1. Processing of scintillation events

The ism binary files, obtained from the SCINDA receiver stations, were processed using the Parseismr.exe programme developed by the suppliers of the Novatel GSV4004B scintillation receivers (Van Dierendonck, 2009). At extraction level, we fixed the lower and upper scintillation thresholds at 0.10 and 1.20 respectively, for filtering out S4 and σ_Φ values. Scintillation levels below 0.10 were considered to be due to background and receiver noise, while those above 1.20 were regarded as outliers (Amabayo et al., 2014). The output generated was recorded after every 60 s interval. Depending on the impact of scintillation events on GPS signals as the signals traverse the ionosphere, scintillation events have been classified into three levels: weak for S4 and σ_Φ values between 0.10 and 0.25, moderate for S4 and σ_Φ values between 0.25 and 0.70 and strong for S4 and σ_Φ values above 0.70 (Jakowski et al., 2008; Kai et al., 2019); and they noted that signal fading peaked when S4 and σ_ϕ values were $\geqslant 0.70$. This classification of scintillation events was adopted in this study and therefore, any scintillation event having S4 and σ_Φ values greater than 0.70 was considered to be a severe scintillation event, capable of causing cycle slips or LL in carrier phase measurements. The monthly percentage occurrence of S4>0.70 or $\sigma_\Phi > 0.70$ or both S4 and $\sigma_\Phi > 0.70$ were calculated using the expression,

Table 1
IGS and SCINDA receiver stations used in this study.

Station	Manufacturer	Receiver	Geographic		Geomagnetic	2011 Days	Resolution
Code	Name	Type	Lat (°)	Lon (°)	Lat (°)	with data	(s)
IGS							
RCMN	LEICA	GRX1200GGPRO	−1.22	36.89	−10.82	331	30
MBAR	ASHTECH	TRE−G3TH	−0.60	30.74	−11.00	158	30
EBBE	TRIMBLE	NETRS	0.04	32.44	−10.07	365	15
SCINDA							
UON	NovAtel	GSV4004B	−1.28	36.82	-10.90	351	60
MBA	NovAtel	GSV4004B	−0.62	30.66	−11.03	80	60
MAK	NovAtel	GSV4004B	0.35	32.57	−9.71	219	60

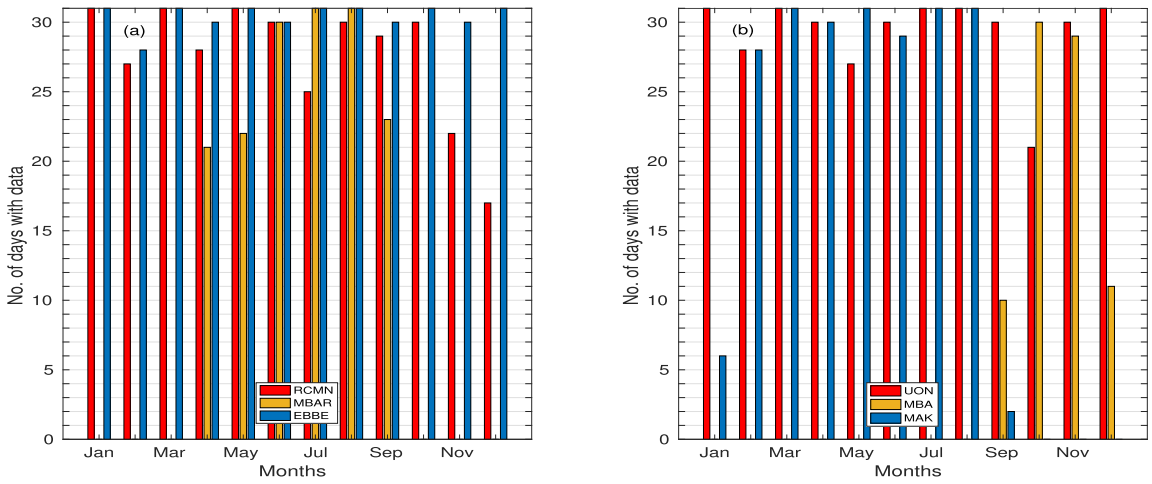


Fig. 2. Monthly number of days with data in 2011 for the (a) IGS stations and (b) SCINDA stations.

Percentage occurrence of scintillation events

$$= \frac{N(X_i)}{N_{Total}} \times 100\%, i = 1, 2, 3., \quad (3)$$

where X_1 stands for S4>0.70, X_2 stands for $\sigma_\phi > 0.70$, and X_3 stands for both S4 and $\sigma_\phi > 0.70$. $N(X_1)$, $N(X_2)$ and $N(X_3)$ stand for the monthly number of data points corresponding to scintillation index S4 > 0.70, scintillation index $\sigma_\phi > 0.70$ and both scintillation indices S4 and $\sigma_\phi > 0.70$ N, respectively. N_{Total} is the total number of scintillation events above noise-level threshold of 0.10 in the month being considered.

To minimize potential multipath and line-of-sight signal obstruction effects, consideration was only given to scintillation events for the ray paths that had elevation angles above 20°. This elevation angle was arrived at given that the GPS receiver stations considered in this study are located in raised semi-arid landscapes where green vegetation cover is minimal. We were also interested in receiving data from as many visible satellites as possible. Thus, setting an elevation angle threshold of 20° was considered to be sufficient to eliminate all the multipath effects as suggested by Amabayo et al. (2014). In addition to the consideration of the elevation angle, signal scintillation events associated with ray paths to GNSS satellites with Pseudo-Random Number (PRN) values beyond 32 were removed. Such satellites were associated with Geostationary Satellite Data and with GNSS constellations other than GPS, according to information obtained from the GPS data scripts.

2.2. Processing of cycle slips

To obtain the carrier-phase measurements from GPS RINEX observation files, we used a MATLAB customized function that outputs the L-band carrier phase measurements L1 and L2 at frequencies f_1 (1.5754 GHz) and f_2 (1.2276 GHz), respectively at a sampling rate of 30 s. Various methods of detecting cycle slips from the L-band carrier measurements have been described by Hofmann-Wellenhof et al. (2007) and Zhen (2012). Such methods include phase and code range combinations, phase combinations, differentials of phases with respect to time, and doppler integration. In this study, we used the method of phase combinations to detect cycle slips on the L-band carrier phase measurements. This method is good for standalone receivers and does not require prior knowledge of the receiver station or spacecraft position coordinates (Gunter, 2003). From the linear combination of the two L-band carrier frequencies f_1 and f_2 with carrier phase pseudoranges Φ_1 and Φ_2, the ionospheric residual, IR, is defined as (Hofmann-Wellenhof et al., 2007),

$$IR = \Phi_1 - \frac{f_1}{f_2}\Phi_2, \quad (4)$$

Eq. (4) shows that IR depends only on the ionosphere and the frequencies of the carrier signals, but is neither dependant on the location of the receiver station nor the satellite position. In the absence of signal scintillation events and cycle slips along the ray paths, the temporal variations of IR would be small. Therefore, sudden jumps in successive values of IR are indicators of cycle slip events that occur simultaneously on both L1 and L2 carrier phases. We used a MATLAB code to search for and to separately count the cycle slips, Y_1, on carrier phase L1 and the cycle slips, Y_2, on carrier phase L2. Our findings revealed that $Y_2 > Y_1$. This meant that the cycle slips were not always occurring simultaneously on both carrier phases. Based on the algorithm proposed by Hofmann-Wellenhof et al. (2007), the cycle slips, Y_3, that occurred simultaneously on both carrier phases, L1 and L2, were searched and counted by observing sudden jumps in the values of IR derived using Eq. (4). To normalize our observations, the total number of cycle slips observed on a specific carrier phase or simultaneously on both carrier phases were expressed as a percentage of all the cycle slips observed in a particular IGS receiver station using the expression,

$$\text{Percentage of cycle slips observed} = \frac{N(Y_i)}{N_{Total}} \times 100\%, \quad i = 1, 2, 3., \tag{5}$$

where Y_1 represents a cycle slip on only carrier phase L1, Y_2 represents a cycle slip on only carrier phase L2 and Y_3 represents simultaneous cycle slips on both carrier phases L1 and L2. $N(Y_1)$, $N(Y_2)$ and $N(Y_3)$ are the total monthly number of cycle slips observed on only L1 phase, only L2 phase and simultaneously on both L1 and L2 phases, respectively. N_{Total} is the total number of cycle slips observed in a given station over a specified time, namely one year.

2.3. Processing of GPS receiver position measurement errors

To analyze the effect of ionospheric scintillation events on the performance of GNSS applications in receiver position measurements, we based our analysis on a comparative study of two consecutive days. We considered a day when ionospheric scintillation events were observed followed by a day when no ionospheric scintillation events were recorded. Although there is no guarantee that scintillation events will not occur the day after an intense scintillation event day, there is also a possibility that the converse is true. Therefore in the interest of this study, we searched for consecutive days; one with scintillation events and the next without scintillation events. The purpose of selecting successive days is to ensure that almost the same satellites were visible in the sky and that their geometry would not have changed greatly on those days. This ensured uniformity of the data sources, thus minimising errors attributed to the malfunctioning of satellite software and/or hardware. To achieve these, satellite positions in the sky were tracked using information obtained from SP3 ephemeris files downloaded from http://earth-info.nga.mil/GandG/sathtml/sp3format.html. These positions were transformed from the earth-centered-earth-fixed (ecef) coordinate system to the local azimuth-elevation-slantrange (AER) spherical coordinate system using the MATLAB in-built function ecef2aer. The AER coordinates were then used to generate the skyplots of the visible satellites at ionospheric pierce point (IPP). The actual SCINDA receiver positions were read from the ism binary files, while the estimated epoch by epoch receiver longitudes, latitudes and altitudes were obtained from PSN files contained in GPS ionospheric scintillation and TEC measurement (GISTM) data, obtainable at the locations of the SCINDA receivers. The difference between the estimated receiver positions and the actual position of the receiver were computed to determine the receiver position measurement errors. Deviations of the estimated receiver positions along longitudes, latitudes and altitudes from the actual receiver position were then converted into arc lengths on the spherical surface of the Earth to obtain the receiver position errors on the Earth's surface along these dimensions in units of length. The standard deviation in the error of the estimated position of each receiver was then determined.

3. Results and discussion

3.1. Signal scintillation

The diurnal occurrence of amplitude scintillation (S4) events derived using scintillation data obtained from the three SCINDA receiver stations of MBA, MAK and UON during the year 2011 is presented in Fig. 3. It is observed that significant scintillation events were registered in all the three receiver stations from 16:00 to 24:00 UT (LT = UT + 3 h), although signal scintillation events were likely to occur at anytime of the day.

These figures clearly show that significant signal scintillation events over the East African region are predominantly post sunset, pre sunrise events. Since the GPS receivers considered in this study are located in raised semi-arid landscapes where green vegetation cover is minimal, it was considered that setting signal ray path elevation angle threshold of $\geqslant 20°$ was sufficient to elliminate all signal scintillation events due to multipath and line-of-sight signal obstructions caused by vegetation cover and landscape terrain as contained in Amabayo et al. (2014). Therefore, the observed post sunset, pre sunrise scintillation events of the GPS L-band navigation signals were a result of ionospheric irregularities (Martiningrum et al., 2013). This region of study is primarily located within the equatorial regions of East Africa, which is mainly characterized by a high diurnal humidity, especially during the equinox months. The observed day time signal scintillation events could thus be attributed to tropospheric effects such as Atmospheric Gravity Waves (AGW) as observed in Amabayo et al. (2015) in Fig. 5(a), (b) and (c). These day time scintillation events could not be attributed to ionospheric irregularities because the latter are predominantly post sunset, pre sunrise events. The intense post sunset ionospheric irregularities which characterize the ionosphere over the East African region is due to the low magnetic dip angle, which favours the onset of Raleigh-Taylor instability (RTI) mechanism. This mechanism is developed whenever plasma with a higher electron density is supported by plasma with a lower electron density (Dungey, 1956). These ionospheric irregularities over the equatorial region were described by Perkins (1975) as small-scale structures in the equatorial ionosphere, which are generally oriented to rapid plasma density fluctuations across the geomagnetic field lines. These ionospheric irregularities have been characterized with respect to solar and geomagnetic activities, seasons, and geographic locations (Fejer et al., 1999; Huang et al., 2002; Lee et al., 2005; Manju et al., 2007; Amabayo et al., 2014). When GPS radio signals traverse these ionospheric irregularities, the signals may be subject to ionospheric scintillation. The degree to which the ionospheric irregularities result in signal scintillation events is determined by the frequency of the incident radio signal

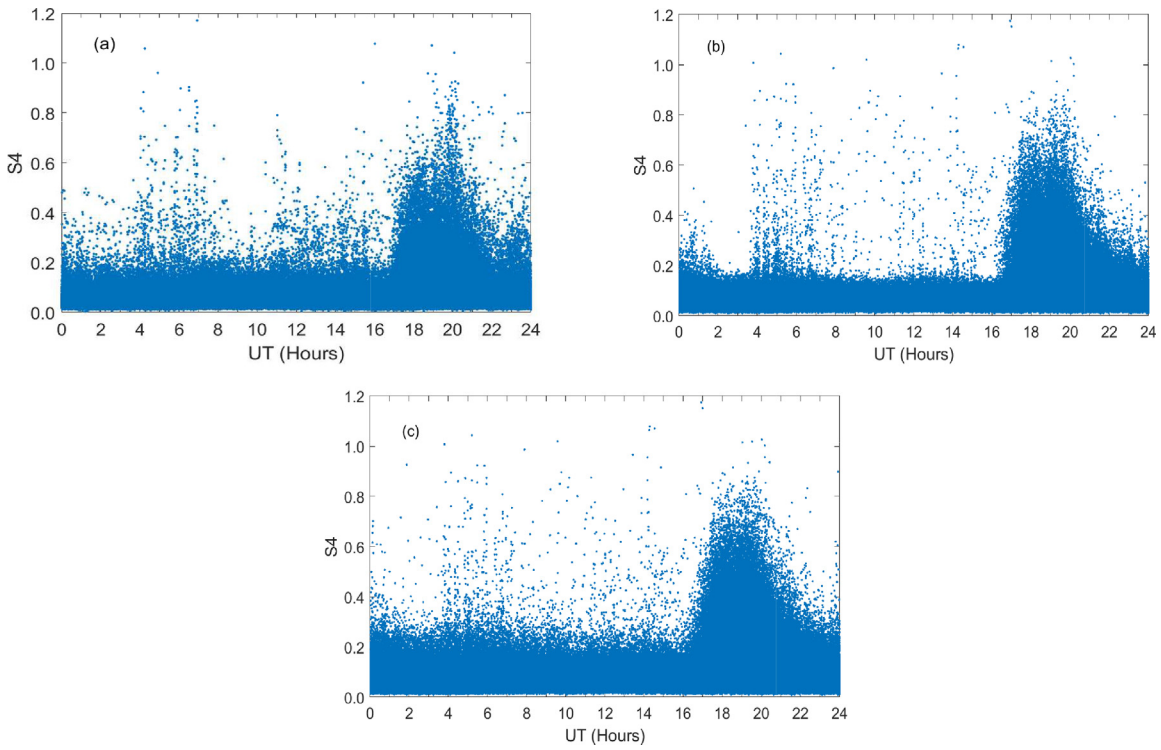


Fig. 3. Cummulative diurnal variation of amplitude scintillation (S4) occurrence over SCINDA station (a) MBA, (b) MAK and (c) UON for the year 2011.

compared to the plasma frequency and the magnitude of the irregularities (Kintner et al., 2007). Radio signals with frequencies below 3 GHz do experience scintillation events and the magnitude of the scintillation effect increases with decrease in the frequency of the radio signal. In particular, Fremouw et al. (1978) noted that significant disruption of navigation systems were produced by the post sunset ionospheric irregularities.

Fig. 4(a), (b) and (c) present the monthly percentage occurrence of amplitude or phase or both amplitude and phase scintillation events over SCINDA receiver stations of MBA, MAK and UON, respectively. The percentage occurrence of the different scintillation events were computed using Eq. (3). In all the three SCINDA receiver stations presented in Fig. 4, the percentage occurrence of amplitude scintillation, S4, without phase scintillation, σ_ϕ, was much higher than that of σ_ϕ occurring without S4. For example, in September 2011 over the SCINDA receiver station MBA, the highest percentage occurrence of amplitude scintillation without phase scintillation was 8.8% while the highest percentage occurrence of phase scintillation without amplitude scintillation was 1.2% for the same period. The corresponding percentage occurrences over MAK for the same period were 10.0% and 0.8% while that over UON were 7.6% and 0.1%, respectively. This trend of the percentage occurrence of amplitude scintillation events being higher than that of phase scintillation events can be seen in all the months of the year 2011. These show that over the East African region, amplitude scintillation events predominate phase scintillation events. This is contrary to what is observed in the high latitudes of Sub-Antarctica region, where phase scintillation events were much more frequent compared to amplitude scintillation events (Kai et al., 2017). Ionospheric irregularities in the high latitudes are driven by precipitation from solar winds that penetrate the polar regions through the open topology of the magnetic fields while in low latitude ionosphere, the irregularities are driven by electrodynamic forces (Aarons et al., 1996; Strangeways et al., 2011). These plasma irregularity sources have different effects on plasma drift velocities. The solar winds induce very high plasma drift velocities at the high latitude regions, which result in very short plasma irregularity scale lengths. In low latitude regions, the electrodynamic forces induce relatively slower plasma drift velocities with fairly longer scale lengths of plasma irregularities. The different length scales of plasma irregularities have got varied impact on the L-band GPS navigation signals (Kelley et al., 1981; Singh et al., 1997). Forexample, in the high latitude regions, the short plasma scale lengths of plasma irregularities cause the refractive effects on the propagating radio signals to dominate while the low latitude regions are dorminated by diffractive effects on the radio signals due to the long scale plasma irregularities. The effects of the scale lengths of the plasma irregularities on the signals can be recorded by ground-based GPS receivers as amplitude or phase scintillations if the satellite and/or the ionosphere move relative to the SCINDA receiver. This may account for the predominance

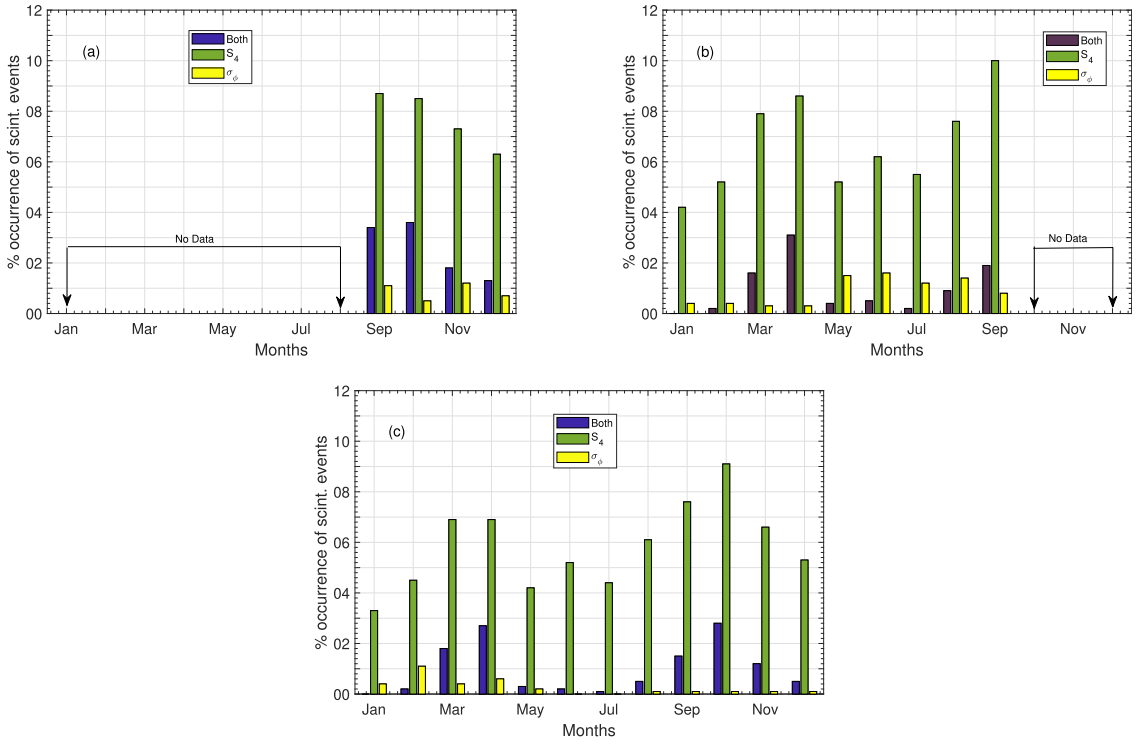


Fig. 4. Percentage (%) occurrence of both S4 and $\sigma_\phi > 0.70$ or only S4>0.70 or only $\sigma_\phi > 0.70$ over SCINDA station (a) MBA, (b) MAK and (c) UON for the year 2011.

of amplitude scintillation over the East African low latitude region compared to the phase scintillation that is predominant in high latitudes.

Further analysis of Fig. 4(b) and (c) reveal that the percentage occurrence of the dominant amplitude scintillation (S4) events peak in the months of March-April and then September-October (equinox months). For receiver station MAK, the highest percentage occurrence of amplitude scintillation events was 10.0% in the September-October period and then 8.8% in the March-April period. The corresponding values for station UON were 9.2% and 6.9%, respectively. Meanwhile, amplitude scintillation (S4) events recorded the minimum percentage occurrence in the months of May-June and then December-January (solstice periods). The least percentage occurrence of amplitude scintillation (S4) events for station MAK in the period of May-June was 5.2% and in December-January it was 4.2%. For data obtained from UON, the corresponding values were 4.2% and 3.3%, respectively. These results show that the predominant amplitude scintillation (S4) events have a seasonal pattern of variation over the East African region (Olwendo et al., 2013). In both stations, it was observed that the percentage occurrence of amplitude scintillation was higher during the September-October equinox than during the March-April equinox. This can be attributed to the fact that the solar terminator for the receiver stations is almost aligned parallel to the geomagnetic flux tubes during equinox since the Solar zenith angle of the receiver stations is then approximately equal to zero (Tsunoda, 1985). In addition, during equinox months more ionization takes place in low latitude ionosphere during the day since the Sun is directly overhead. Therefore, due to PRE, which sets off at dusk, the vertical thrust ($\vec{E}x\vec{B}$) on plasma is greatly strengthened. This creates a conducive environment for the RTI-mechanism, which leads to the developement of ionospheric irregularities that can cause signal scintillations.

3.2. Occurrence of cycle slips

When GNSS navigation signals traverse ionospheric irregularities, the signals may be subject to ionospheric scintillation events. Previous studies (e.g. Jakowski et al., 2008; Kai et al., 2019) suggested that discontinuities in tracked GNSS navigation signals were associated with strong scintillation events (S4>0.70) and that these disconitinuities may result in the PLL of a GNSS receiver losing track of the signal. However in Fig. 5(a.1), when scintillation events (S4>0.50) were recorded at satellite elevation angles >25° from 17:45 to 18:30 UT, it was observed in Fig. 5(a.2) that there were no discontinuities in the tracked signal. Interestingly, when weak and moderate scintillation events (S4<0.40) were registered between 18:30 and 20:10 UT in Fig. 5(a.1), it is observed in Fig. 5 (a.2) that at the same time interval there were discontinuities in the tracked signal.

Unlike in Fig. 5(a.1), the high scintillation events (S4>0.70) recorded by PRN5 in Fig. 5(b.1) from 18:30 to 20:00 UT resulted in loss-of-lock of the tracked signal as

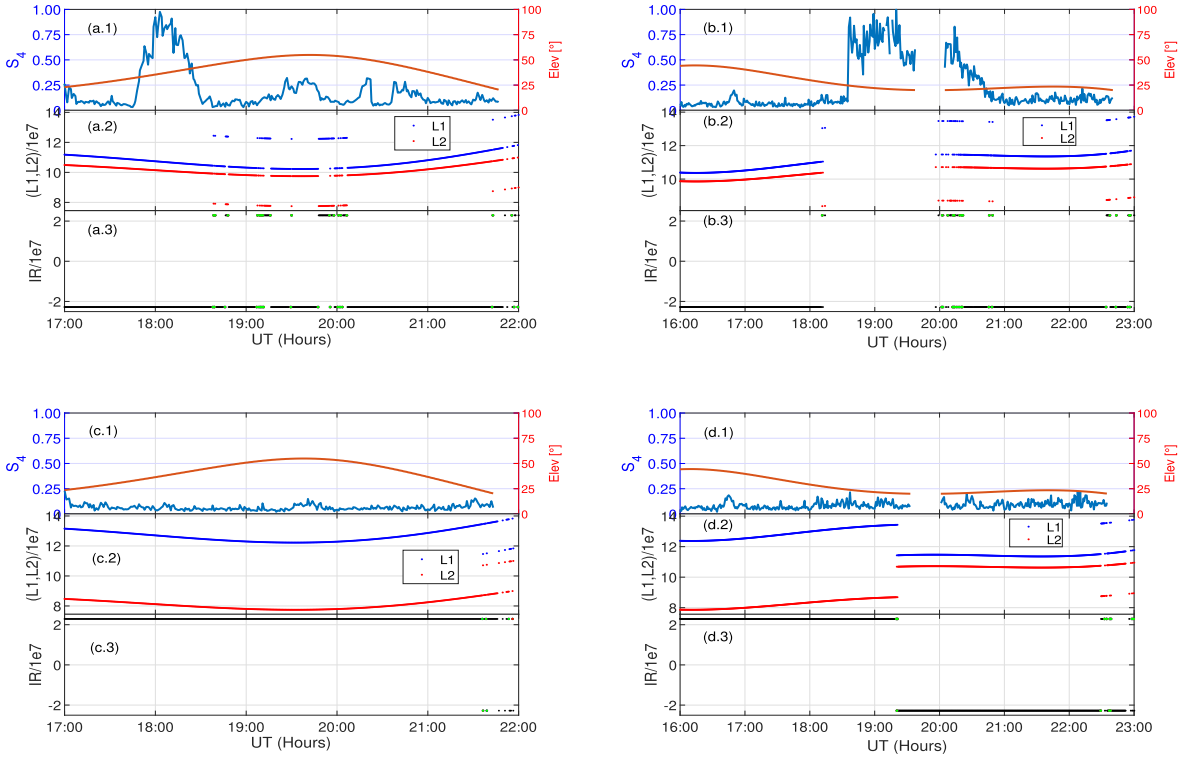


Fig. 5. The MBA SCINDA and MBAR IGS data used in panels (a) and (c) were recorded by PRN2 on 2011-04-05 and 2011-04-06, respectively. While in panel (b) and (d), the MBA SCINDA and MBAR IGS data used were recorded by PRN5 on 2011-04-05 and 2011-04-06, respectively. The panels show satellite elevations, amplitude scintillation events, cycle slips and loss-of-lock events.

shown in Fig. 5(b.2). The data gap observed from PNR5 in the MBA SCINDA data on day 2011-04-05 between 19:38 and 20:05 UT as shown in panel (b.1) occurred at the same time on day 2011-04-06 as shown in panel (d.1). This data gap is not associated with the scintillation. Since the data gap occurred when the ray path elevation dropped below 20 degrees, it was probably due to a masking of the ray path by some structure in the environment of the antenna. Therefore, existence of cycle slips in tracked signal paths may not necessarily reflect the presence of strong scintillation events. However, the frequency of occurrence of cycle slips on either L1 or L2 or both do seem to correspond to increased ionospheric scintillation events. On 2011-04-06, only weak scintillation events (S4<0.20) were registered as shown in Fig. 5(c.1) and Fig. 5(d.1) using SCINDA data recorded from PRN2 and PRN5, respectively, by GPS SCINDA receiver MBA. Fig. 5(c.1) suggests that in the absence of scintillation events, no cycle slips were observed in the tracked signal. Those that appeared in the tracked signal after 20:30 UT were probably due to multipath effects since the satellite elevation angles were very low i.e. <20°. For dual frequency GPS L-band signals, the discontinuities can manifest sudden jumps or data gaps in the tracked GNSS signal. These sudden jumps may occur on either L1 (1.5754 GHz) or L2 (1.2276 GHz) or simultaneously on both of the carrier frequencies. Figs. 5(a.2) and (b.2) demonstrate the occurrence of cycle slips on L1 and L2 carrier frequencies of the GPS L-band as recorded from PRN2 and PRN5, respectively. Note that the jump in L1 carrier frequency is always opposite in direction to the jump in L2 carrier frequency. Using Eq. (4), the IR values were computed to show the sudden jumps in the tracked signal as presented in Figs. 5(a.3), (b.3), (c.3) and (d.3). Note that the sudden jumps in the successive values of IR are to a factor greater than $2x10^7$ cycles and they are indicators of cycle slips Mungufeni et al. (2015). The magnitude of the sudden jumps in L1 and L2 carrier phase measurements shown in Figs. 5(a.2), (b.2), (c.2) and (d.2) are dependent on the GNSS receiver types. Therefore, the IR variations are also different between GNSS receiver types. Moreover, since an initial value of IR index depends on the initial values of the carrier phase observations L1 and L2, known as the integer biases, the absolute value of IR does not reflect actual value related to ionospheric effects. In the absence of scintillation events, the temporal changes in the successive values of IR are very small and thus approximately appear as straight lines shown intermittently in Figs. 5(a.3), (b.3), (c.3) and (d.3) as black lines. The green points/lines on the black lines in Figs. 5(a.3), (b.3), (c.3) and (d.3) represent moments where cycle slips occurred simultaneously on both L1 and L2 carrier frequencies. In Fig. 5, the search for the occurrance of cycle slips and LL was limited between 16:00 to 23:00 UT in order to increase the chances of observing cycle slips since at this time interval, the ionosphere over the East African region is more turbulent due to electrodynamic forces.

However, due to day time tropospheric scintillation events over the region of study, occurrence of cycle slips during the day could not be ruled out. These cycle slips may pose serious threats to safety if the signal discontinuities result in an increase in position measurement error, which is detrimental to GNSS navigation applications.

In Fig. 6(a) we present the annual percentage occurrence of cycle slips on the L-band frequencies registered by the IGS receivers under consideration. In general, signal tracking performance differs depending on the receiver types. Hence even if there were identical scintillation intensity levels at the three sites, there might be differences in the cycle slip occurrence. However, the general trend observed was that the annual percentage occurrence of cycle slips on the L2 frequency of the L-band was higher than that of cycle slips occurring on either L1-frequency or on both L1 and L2 frequencies concurrently. These annual percentage occurrence of cycle slips were computed using Eq. (5). Quantitatively, the annual percentage occurrence of cycle slips on L1-frequency computed using data obtained from IGS receiver station MBAR was 37% while that on L2-frequency was 39%, and on both L1 and L2 frequencies concurrently it was 24%. For the GPS receiver station EBBE, the corresponding values were 45%, 55% and 2%, respectively. While for the GPS receiver station RCMN, the corresponding values were 34%, 44% and 18%, respectively. The magnitude at which a navigation signal experiences scintillation events is inversely related to the frequency of the signal and directly proportional to the strength of the signal (Kintner et al., 2007). Typically, L2-signal has an amplitude that is 10 dB below that of the L1-signal. Thus, the higher frequency signal (L1) experiences less scintillation effects than the lower frequency (L2) signal. Consequently, more cycle slips would occur on the L2-frequency than on the L1-frequency. At both stations, the percentage for the simultaneous occurrence of cycle slips in both L1 and L2 frequency bands was low. This implies that the percentage occurrence of cycle slips on an individual L-band frequency is higher than that of cycle slips occuring simultaneously on both L-band frequencies.

The monthly percentage occurrence of cycle slips as registered by the three IGS stations is presented in Fig. 6(b). Firstly, it shows that the monthly percentage occurrence of cycle slips follow a seasonal pattern. Even though the signal tracking performance differs depending on the receiver types, all the three IGS stations showed that the occurrence of cycle slips were more frequent in the equinox months than in the solstice months. This could be attributed to the strong ionospheric irregularities that exist during equinox compared to solstice (Tsunoda, 1985). Secondly, the cycle slips are seen to occur more frequently in the western side of East Africa than on the eastern side. For example, in September, IGS station MBAR, which is further west in the region, registered about 33% occurrence of cycle slips. This was followed by IGS station EBBE with 23% occurrence of cycle slips. The station that registered the least percentage occurrence of cycle slips was RCMN with 20% and it is located more to the eastern side of the region. As explained by Abiriga et al. (2020), more ionospheric irregularities occur in the western side of East Africa than on the eastern side. This is because the eastern side has an increased geomagnetic field strength compared to the western side. According to the RT-plasma growth rate equation, the vertical component of plasma drift velocity increases with a decrease in the geomagnetic field strength. Consequently, more severe ionospheric irregularities will occur in the western side of the region than to the eastern side. This explains the existence of more cycle slips in the western side of the region. This also implies that the occurrence of cycle slips in a region is affected by the strength of the geomagnetic field in the region.

3.3. Effect of ionospheric scintillations on GPS receiver position measurements

GPS satellite paths tracked for two consecutive days (2011-04-05 and 2011-04-06) from 19:00 to 19:30 UT are presented in Fig. 7(a) and (b). These polar plots present a sky view of the visible satellites over the MAK SCINDA receiver station. The satellites were tracked using data obtained from the PSN files. The center of the polar plots

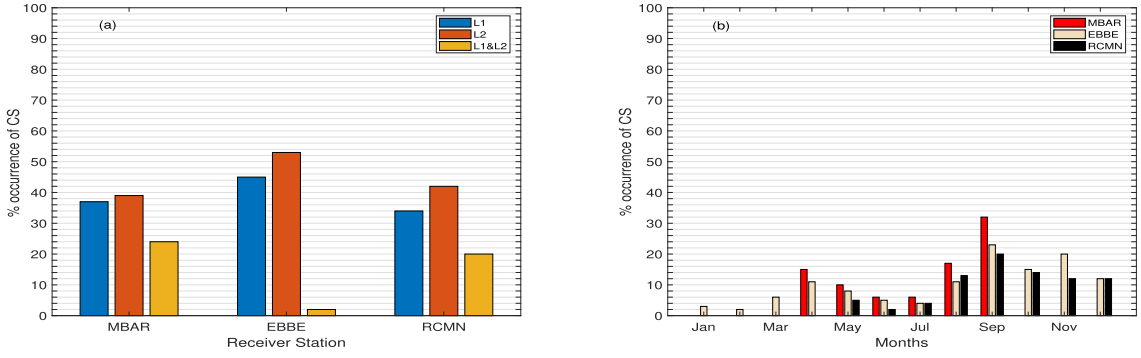


Fig. 6. (a) Annual percentage occurrence of cycle slips on L1, L2 or both phases of L-band over MBAR, EBBE and RCMN. (b) Monthly percentage occurrence of cycle slips over MBAR, EBBE and RCMN in the year 2011.

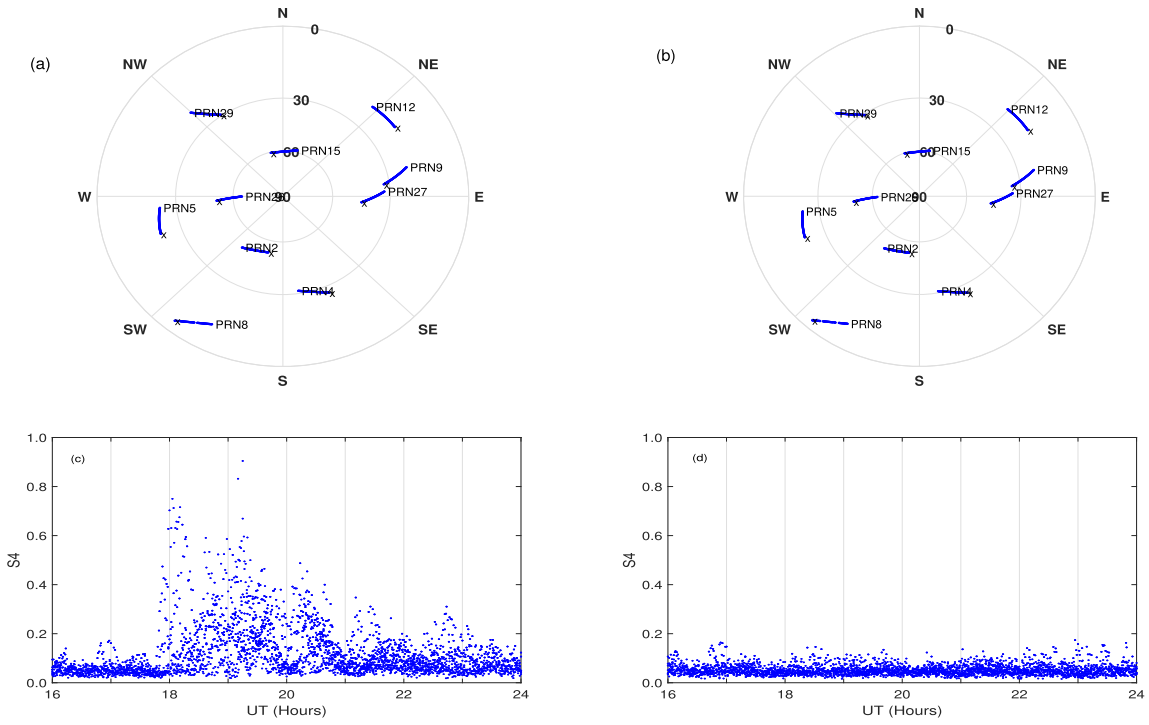


Fig. 7. (a) and (b) Polar plots of visible satellites in azimuth-elevation coordinates at ionospheric pierce point (IPP) over MAK between 19:00 and 19:30 UT on 2011-04-05 and 2011-04-06, respectively. The 'x' at the end of the satellite path indicates the direction in which the satellite is travelling. (c) and (d) indicate signal scintillation (S4) events derived from scintillation data obtained from all PRNs visible by SCINDA receiver station MAK between 16:00 and 24:00 UT on the respective days.

are the local zenith of the SCINDA receiver station and the surrounding equally-spaced circular contours represent different elevation masking angles. On these consecutive days, the polar plots show that the same satellites were visible in the sky over the MAK SCINDA receiver station. The visible satellites were those with pseudorandom noise (PRN) numbers 2, 4, 5, 8, 9, 12, 15, 26, 27 and 29. It should also be noted that these satellites were approximately in the same locations during the two consecutive days presented and hence their geometry remained fairly constant. We thus used the scintillation data obtained from the MAK SCINDA receiver station to plot the variation of registered signal amplitude scintillation (S4) events against time as shown in Fig. 7(c) and (d). Fig. 7(c) shows that moderate signal scintillation events ($0.25<S4<0.70$) were observed on 2011-04-05 between 17:45 and 20:15 UT. Only a few severe signal scintillation events ($S4 > 0.70$) were registered on that day. It is visible in Fig. 8(a) that at the onset of signal scintillation events ($S4 \geqslant 0.25$) at about 17:45 UT, the number of visible satellites began to fluctuate rapidly. Between 18:00 to about 19:00 UT, the number of visible satellites is observed to fluctuate between ten to eight. However, between 19:00 to 20:00 UT, the number of visible satellites fluctuated between nine and seven. It must be noted in Fig. 7(c) that the signal scintillation events were observed to be more frequent between 19:00 to 20:00 UT than between 18:00 to 19:00 UT.

Meanwhile, on 2011-04-06 only mild signal scintillation events ($S4<0.25$) were recorded as shown in Fig. 7(d). Consequently, the number of visible satellites remained fairly constant between ten and nine for most of the time on 2011-04-06 as shown in Fig. 8(b). Therefore, Figs. 7(a) and (b), and Figs. 8(a) and (b) show a direct correlation between the occurrence of scintillation events and the variation in the number of visible satellites. The variability in the number, and hence geometry, of visible satellites can affect the performance of GNSS applications since a reduced number and poor geometry of visible satellites can lead to high dilution of precision (DOP) values that can translate into significant errors in GPS position measurements (Spilker, 2016). These errors limit the accuracy and reliability of GNSS applications in navigation and mapping. To demonstrate this, we present Figs. 8(c) and (d) to show the variation with time of the estimated SCINDA receiver station positions obtained from the PSN files. The region of interest in Fig. 8(c) begins from 18:00 to 20:00 UT, when signal scintillation events were observed on 2011-04-05. The receiver station position measurement errors can manifest in three dimensions (along the longitude, latitude and altitude). These errors are presented in the metric unit of distance in Fig. 8. $\Delta x, \Delta y, \Delta h$ and Δr represent errors along the longitude, latitude, altitude and the three dimensional (3D) error in the receiver position, respectively. By comparison, on 2011-04-05, the value of $\Delta x = 4$ m, $\Delta y = 6$ m, $\Delta h = 11$ m and $\Delta r = 13$ m while on 2011-04-06, the values of $\Delta x, \Delta y, \Delta h$ and Δr were all less than 2 m. On 2011-04-05, the least error (4 m) in the measurement of the receiver position was along the lon-

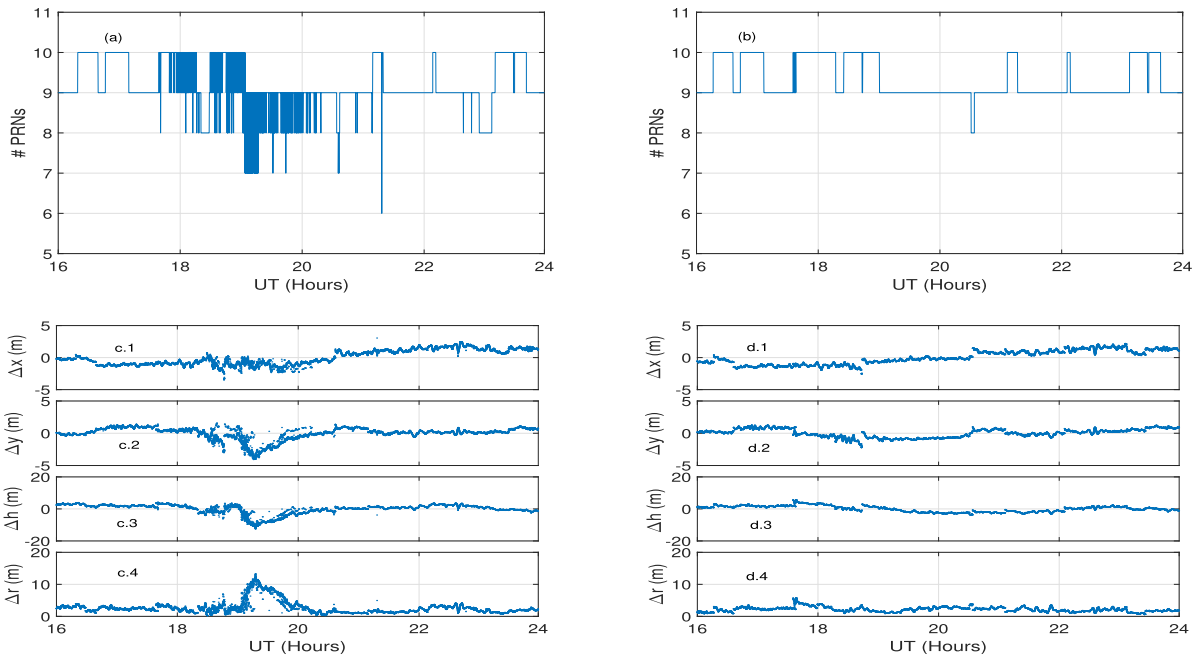


Fig. 8. (a) and (b) show the variation in the number of visible GPS satellites obtained from GISTM data for SCINDA receiver station MAK on 2011-04-05 and 2011-04-06, respectively. While (c) and (d) show the time series of the position of the GPS SCINDA receiver station MAK from GISTM data on the respective days.

gitude while the maximum error (11 m) was along the altitude; $\Delta r = \sqrt{\Delta x^2 + \Delta y^2 + \Delta h^2}$. The vertical error distances shown in Fig. 9(c.3) were measured from sea level. In the same time interval, Fig. 8(d.1), (d.2), (d.3) and (d.4) do not show significant errors in position measurements for day 2011-04-06 due to the absence of signal scintillation events. These results show that signal scintillation events can greatly affect the accuracy of GNSS receiver position measurements.

Furthermore, it can be deduced from Fig. 8(c) that scintillation events shown in Fig. 7(a) with S4 values as low as 0.40 are capable of introducing significant navigation and mapping errors in GNSS applications. From the comparison of Figs. 7 and 8, it is evident that during periods of high occurrence of scintillation (S4) events on some satellite links, there is an increased fluctuation in the number of visible satellites. In addition, Fig. 8 illustrates the coincidence of the fluctuation in the number of visible satellites and the increase in the error of position measurements. This appears to be the case only if the affected navigation signals originate from the satellites used in position measurements. To date, GPS is still the most commonly used navigation system since the standard message format is broadcast on the GPS L1 frequency (GPS L1) to facilitate interoperability from the user's perspective. With SBAS augmentation systems using GNSS data becoming more widely used for aircraft approach-and-landing guidence, and also for awareness and warning against terrain encounters, errors induced by scintillation events in aircraft navigation can increase the uncertainty in the vertical protection levels and deprive the users from the GPS accuracy required for precision approach landing and thus incur delays in landing and additional costs for fuel (https://www.icao.int/APAC/Documents/edocs/SBAS%20safety%20assessment%20guidance.pdf). Although the scintillation effects are related to availability and continuity of the GNSS augmentation systems for aircraft navigation, we point out that augmentation of GNSS positioning is mainly available near airports. The position estimates for the rest of the flight is derived from L1 position estimates, of which the errors are likely to be larger than the errors logged in the psn-files. The position estimates in the psn files are derived from both the L1 and L2 signals. For example, between November 1998 and February 1999, 11.5% of flight crew errors that resulted in fatal aircraft accidents were attributed to GNSS navigation errors (Jean-Pierre, 1999). About 71% of all the GNSS position measurement errors are associated with ionospheric scintillation events resulting from ionospheric irregularities (Dhiraj, 2013). Thus, the accuracy and realiability of position measurements obtained from GNSS applications can be compromised by scintillation events in signal ray paths.

On 2011-04-05 when signal scintillation events were observed, the horizontal spread of the estimated receiver positions occupied a latitude by longitude area of 0.000052° by 0.000053°, with a larger spread of the position estimates appearing to the West than to the East of the actual receiver position as shown in Fig. 9(a). However, on 2011-04-06, the spread of the estimated receiver position estimates occupied a small area of the latitude by longitude scale (0.000032° by 0.000042°) as shown in Fig. 9(b). The skewing of the estimated receiver positions can be

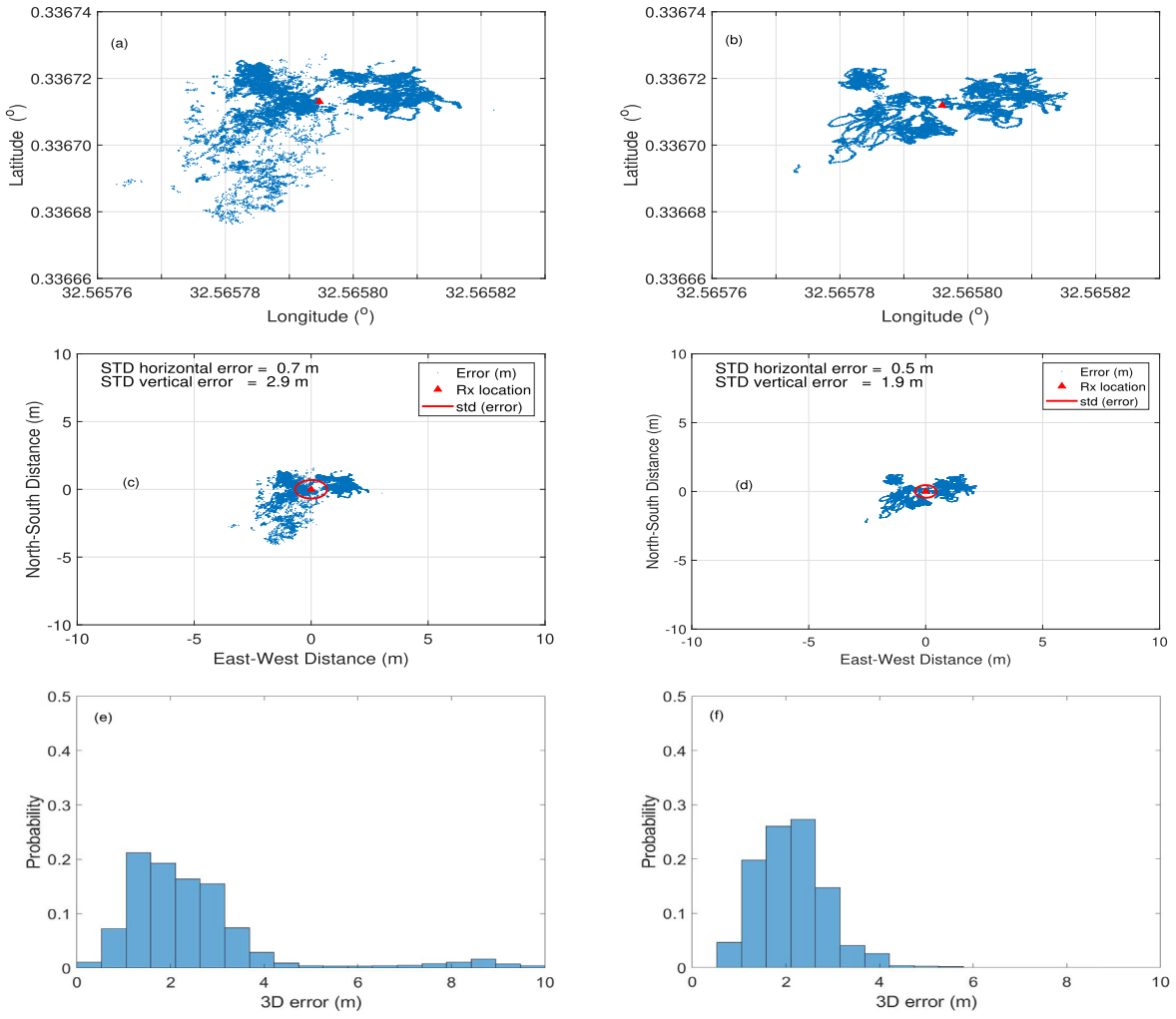


Fig. 9. (a) and (b) Time series of horizontal position measurement errors of the IGS receiver EBBE between 17:45 and 18:15 UT on 2011-04-05 and 2011-04-06, respectively. (c), (d), (e) and (f) present the spread of the position measurement errors on latitude/longitude scale on the respective days.

explained by the fluctuations in the number and geometry of the satellites that were in view between 19:00 and 19:30 UT as shown in Fig. 8(a) and (b). In Fig. 9(c) and (d), the standard deviation of the errors in the receiver position measurements along the horizontal and vertical directions are presented for 2011-04-05 and 2011-04-06, respectively. The respective standard deviations in the receiver position measurement errors were greater on 2011-04-05 by 0.2 m and 1.0 m along the horizontal and vertical dimensions compared to those measured on 2011-04-06. The distribution of these position measurement errors in terms of the probability of occurrence is presented in Fig. 9(e) and (f), respectively. Fig. 9(e) shows that there are chances of getting position measurement errors of up to 10 m on 2011-04-05 while on 2011-04-06 it stands at 5 m. The correlation between high S4 and the corresponding increase in the fluctuations of the position estimates (Figs. 8 (c) and (d)) provide sufficient evidence for the increase in the position errors observed in Fig. 9. The increased position errors are a result of the high rate of fluctuation in the number of visible satellites used by the receiver in position calculations. This explains the fact that the decrease in the number of visible satellites changes the geometry of the satellites used for positioning, which results in an increase in the dilution of precision. All these demonstrate that the presence of scintillation events in signal ray paths compromise the accuracy and reliability of GNSS applications in position measurements.

4. Conclusions

Using available GPS and SCINDA data recorded at three IGS and three co-located SCINDA receiver stations in the year 2011, we have investigated the impact of signal scintillation events on the performance of GNSS applications over the East African region in terms of cycle slip occurrence, loss-of-lock and position measurement error. We observed that;

1. The GNSS signals that traverse the East African ionosphere may be subject to both amplitude and phase scintillation events. However, the frequency of occurrence of amplitude scintillation events is greater than that for phase scintillation events.
2. Although signal tracking performance differs depending on the receiver types in general, the frequency of occurrence of cycle slips was observed to be dependent on the carrier frequency of the GPS L-band signal. Thus, the frequency of occurrence of cycle slips was observed to be higher on the L2-frequency of the L-band than on the L1-frequency.
3. The occurrence of cycle slips was more frequent to the western side of East Africa (Lon $\sim$ 29°) than to the eastern side of the region (Lon $\sim$ 41°). This revealed an inverse relation between the occurrence of cycle slips and geomagnetic field strength since the magnitude of the magnetic field strength in the western side is less than that in the eastern side of the region at the same geographic latitudes.
4. The presence of ionospheric scintillation affected the GNSS position measurements in the region by increasing the position error as estimated from dual frequency GPS data up to 10 m. This compromised the accuracy and reliability of GNSS applications for navigation and surveying.

Declaration of Competing Interest

The authors declare that they have no known competing financial interests or personal relationships that could have appeared to influence the work reported in this paper.

Acknowledgement

We acknowledge the financial support from the International Science Programme (ISP) of Uppsala University in Sweden. The first author acknowledges the administration and staff of the South African National Space Agency (SANSA) for the support during his research visit to the institution. Special thanks to the Crustal Dynamics Data Information System (cddis) data Centre from where the GPS data was downloded. We also acknowledge Makerere University, Mbarara University of Science and Technology, and University of Nairobi for providing the scintillation data used in this study collected from SCINDA receivers provided by the Air Force Research Laboratory in coordnation with Boston College, USA.

References

Aarons, J., Mendillo, M., Yantoseca, R., 1996. GPS phase fluctuations in the equatorial region during the MISETA 1994 campaign. J. Geophys. Res. 101 (A12), 26851–26862. https://doi.org/10.1029/96JA00981.

Abiriga, F., Amabayo, E.B., Jurua, E., Cilliers, P.J., 2020. Statistical Characterization of Equatorial Plasma Bubbles over East Africa. J. Atmos. Sol. Terr. Phys. 200, 10519. https://doi.org/10.1029/2011RS004846.

Amabayo, E.B., Jurua, E., Pierre, J.C., Habarulema, J.B., 2014. Climatology of ionospheric scintillations and TEC trend over the Ugandan region. Adv. Space Res. 53, 734–743. https://doi.org/10.1016/j.asr.2013.12.015.

Amabayo, E.B., Jurua, E., Pierre, J.C., 2015. Validating the use of scintillation proxies to study ionospheric scintillation over the Ugandan region. J. Atmos. Sol. Terr. Phys. 128, 84–91. https://doi.org/10.1016/j.jastp.2015.03.006.

Banville, S., Langley, R., Saito, S., Yoshihara, T., 2010. Handling cycle slips in GPS data during ionospheric plasma bubble events. Radio Sci. 45. https://doi.org/10.1029/2010RS004415.

Beach, T.L., 2006. Perils of the GPS phase scintillation index (sigma_phi). Radio Sci. 41. https://doi.org/10.1029/2005RS003356.

Briggs, B.H., Parkin, I.A., 1963. On the variation of radio star and satellite scintillations with zenith angle. J. Atmos. Sol. Terr. Phys. 25, 339–365. https://doi.org/10.1016/0021-9169(63)90150-8, Pergamon Press Ltd, Northern Ireland.

Conker, R.S., El Arini, M.B., Hegarty, C.J., Hsiao, T., 2003. Modeling the effects of ionospheric scintillation on GPS/SBAS availability. Radio Sci. 38 (1), 1001. https://doi.org/10.1029/2000RS002604.

Datta-Barua, S., Doherty, P.H., Delay, S.H., Dehel, T., Klobuchar, J.A., 2003. Ionospheric scintillation effects on single and dual frequency GPS positioning. In: Proceedings of ION GPS/GNNS, Portland, OR, pp. 336–346.

Dhiraj, P., 2013. Estimation of prominent global positioning system measurement errors for GAGAN applications. Eur. Sci. Scitfic J. 9 (15). https://doi.org/10.19044/esj.2013.v9n15p%25p.

Donghyun, K., Langley, R.B., 2001. Instantaneous Real-time cycle slip correction of Dual-frequency GPS Data. In: International symposium of Kinematic Systems in Geodecy, Geomatics and Navigation (KIS2001), Banff, Alberta, Canada, Jun 5–8.

Du, J., Wilkinson, P., Thomas, R., Cervera, M., 2000. Determination of Equatorial Ionospheric Scintillation S4 Dual Frequency GPS. Workshop, La Trobe University, Australia, URSI Commission G.

Dungey, J.W., 1956. Convective diffusion in Equatorial F-region. J. Atmos. Terr. Phys. 9, 304–310. https://doi.org/10.1016/0021-9169(56)90148-9.

Fejer, B.G., Scherliess, L., de Paula, E.R., 1999. Effects of the vertical plasma drift velocity on the generation and evolution of equatorial spread F. J. Geophys. Res. 104, 19859–19870. https://doi.org/10.1029/1999JA900271.

Fremouw, E.J., Leadabrand, R.L., Livingston, R.C., Cousins, M.D., Rino, C.L., Fair, B.C., Long, R.A., 1978. Early results from the DNA Wideband satellite experiment-Complex-signal scintillation. Radio Sci. 13, 167–187. https://doi.org/10.1029/RS013i001p00167.

Gunter, S., 2003. Satellite Geodesy. Walter de Gruyter GmbH Co. KG 10785, Berlin. Universitat Hannover Schneiderberg, 50 30167 Hannover, Germany. ISBN: 3-11-017549-5.

Hofmann-Wellenhof, B., Lichtenegger, H., Wasle, E., 2007. Global Navigation Satellite Systems, GPS, GLONASS, Galileo and More. Springer, Wien, New York, 978-3-211-73012-6.

Huang, C.Y., Burke, W.J., Machuzak, J.S., Gentile, L.C., Sultan, P.J., 2002. Equatorial plasma bubbles observed by DMSP satellites during a full solar cycle: toward a global climatology. J. Geophys. Res. 107 (A12), 2002. https://doi.org/10.1029/2002JA009398.

Humphreys, T.E., Psiaki M.L., Ledvina B.M., and Kintner P.M., 2005. GPS carrier tracking loop performance in the presence of ISs. In: Proc. IONGNSS. Institute of Navigation, Long Beach, CA.

Jakowski, N., Mayer, Ch., Wilken, V., Hoque, M.M., 2008. Ionospheric impact on GNSS Signals. Fisica de la Tierra 20, 11–25.

Jean-Pierre, D., 1999. Flight Safety Foundation; Flight Safety Digest (Approach-and-landing accident reduction task force; Aircraft Equipment Working Group). Final Report, February.

Jiao, Y., Morton, Y., Taylor, S., Pelgrum, W., 2014. Scintillating Statistics: A look at high-latitude and equatorial ionospheric disturbances of GPS signals. J. Atmos. Solar-Terr. Phys. 67, 1074–1084.

Kai, G., Yang, L., Yan, Z., Jinling, W., 2017. Analysis of Ionospheric Scintillation characteristics in Sub-Antarctica region with GNSS data at Macquarie Island. Sensors 17, 137. https://doi.org/10.3390/s17010137.

Kai, G., Marcio, A., Sreeja, V.V., 2019. Ionospheric scintillation intensity fading characteristics and GPS receiver tracking performance at low latitudes. GPS Solut. 23, 43. https://doi.org/10.1007/s10291-019-0835-1.

Kelley, M.C., Larsen, M.F., LaHoz, C., McClure, J.P., 1981. Gravity wave initiation of equatorial spread F: A case study. J. Geophys. Res. 86, 9087–9100. https://doi.org/10.1029/JA086iA11p09087.

Kintner, P., Ledvina, B.M., de Paula, E.R., 2007. GPS and ionospheric scintillation. Space Weather 5, S09003. https://doi.org/10.1029/2006SW000260.

Klobuchar, J.A., 1991. Ionospheric effects on GPS. GPS World 2 (4), 48–51.

Lee, C., Liu, J.Y., Reinisch, B.W., Chen, W.S., Chu, F.D., 2005. The effect of prereversal drift, the EIA asymmetry, and magnetic activity on the equatorial spread F during solar maximum. Ann. Geophys. 23, 745–751. https://doi.org/10.5194/angeo-23-745-2005.

Leick, A., 1995. GPS Satellite Surveying, second ed. John Wiley, Hoboken, N.J.

Leick, A., 2004. GPS satellite surveying, 3rd edn. Wiley, New York Teunissen PJG (1995) The least-squares ambiguity decorrelation adjustment: a method for fast GPS integer ambiguity estimation. J Geodesy 70 (1), 65–82. https://doi.org/10.1007/BF00863419.

Manju, G., Devacia, C.V., Sridharan, R., 2007. On the seasonal variations of the threshold height for the occurrence of equatorial spread F during solar minimum and maximum year. Ann. Geophys. 25 (855–861), 2007. https://doi.org/10.5194/angeo-25-855-2007.

Martiningrum, D.R., Abadi, P., Yokoyama, T., Yamamoto, M., 2013. Relationship between Scintillation and Ionospheric Irregularities over Kototabang. In: Proceedings of the 3rd Research Enhancement and System Establishment for Space Weather in Indonesia.

Mungufeni, P., Jurua, E., Habarulema, J.B., Anguma, S.K., 2015. Modelling the probability of ionospheric irregularity occurrence over African low latitude region. Atmos. Sol. Terr. Phys. 128, 46–57. https://doi.org/10.1016/j.jastp.2015.03.010.

Olwendo, O.J., Baluku, T., Baki, P., Cilliers, P.J., Mito, C., Doherty, P., 2013. Low latitude ionospheric scintillation and zonal irregularity drifts observed with GPS-SCINDA system and closely spaced VHF receivers in Kenya. Adv. Space Res. 51, 1715–1726. https://doi.org/10.1016/J.ASR.2012.12.017.

Perkins, F.W., 1975. Ionospheric irregularities. Rev. Geophys. 13, 884. https://doi.org/10.1029/RG013i003p00884.

Singh, S., Johnson, F.S., Power, R.A., 1997. Gravity wave seeding of equatorial plasma bubbles. J. Geophys. Res. 102, 7399–7410. https://doi.org/10.1029/96JA03998.

Skone, S., Knudsen, K., De Jong, M., 2001. Limitations in GPS receiver tracking performance under ionospheric scintillation conditions. Phys. Chem. Earth Part A 26 (6), 613–621.

Skone, S., Lachapelle, G., Yao, D., Yu, W., Watson, R., 2005. Investigating the Impact of Ionospheric Scintillation using a GPS Software Receiver. In: Presented at the ION GNSS 2005 Conference, September 13–16. Long Beach, CA.

Spilker, J.J., 2016. Satellite constellation and Geometric Dilution of Precision. Am. Inst. Aeronaut. Astronaut., http://arcaiaa.org.

Sreeja, V., Aquino, M., Elmas, Z.G., 2011. Impact of ionospheric scintillation on GNSS receiver tracking performance over Latin America: Introducing the concept of tracking jitter variance maps. Space Weather 9, S10002. https://doi.org/10.1029/2011SW000707.

Strangeways, H.J., Ho, Y.-H., Aquino, M.H.O., Elmas, Z.G., Marques, H.A., Monico, J.F.G., Silva, H.A., 2011. On determining spectral parameters, tracking jitter, and GPS positioning improvement by scintillation mitigation. Radio Sci. 46, RS0D15. https://doi.org/10.1029/2010RS004575.

Tsunoda, R.T., 1985. Control of the seasonal and longitudinal occurrence of equatorial scintillations by the longitudinal gradient in integrated E region Pedersen conductivity. J. Geophys. Res. 90 (A1), 447–456. https://doi.org/10.1029/JA090iA01p00447.

Van Dierendonck, A.J., 2009. GPS Ionospheric Scintillation and TEC monitor. AJ Systems/GPS silicon valley, California, U.S.A. 23 March to 9 April.

Van Dierendonck, A., Arbesser-Rastburg, B., 2004. Measuring Ionospheric Scintillation in the Equatorial Region over Africa, Including Measurements from SBAS Geostationary Satellite Signals. In: Proceeding of the ION GNSS 17th Technical Meeting of the Satellite Division, Long Beach, CA, USA, pp. 21–24.

Yizengaw, E., Retterer, J., Pacheco, E.E., Roddy, P., Groves, K., Caton, R., Baki, P., 2013. Postmidnight bubbles and scintillations in the quiettime June solstice. Geophys. Res. Lett. 40, 5592–5597. https://doi.org/10.1002/2013GL058307.

Yue, X., Schreiner, W.S., Hunt, D.C., Rocken, C., Kuo, Y.-H., 2011. Quantitative evaluation of the low Earth orbit satellite based slant total electron content determination. Space Weather 9, S09001. https://doi.org/10.1029/2011SW000687.

Yue, X., Schreiner, W.S., Pedatella, N.M., Kuo, Y.-H., 2016. Characterizing GPS radio occultation loss of lock due to ionospheric weather. Space Weather 14. https://doi.org/10.1002/2015SW001340.

Zhen, D., 2012. MATLAB software for GPS cycle-slip processing. GPS Solut 2012 (16), 267–272. https://doi.org/10.1007/s10291-011-0249-1.